

## Author's Accepted Manuscript

Chandrayaan-1 X-ray spectrometer (C1XS) –  
Instrument design and technical details

C.J. Howe, D. Drummond, R. Edeson, B. Maddison,  
D.J. Parker, R. Parker, A. Shrivastava, J. Spencer,  
B.J. Kellett, M. Grande, P. Sreekumar, J. Huovelin,  
D.R. Smith, J. Gow, S. Narendranath.K.C., L. d'Uston

PII: S0032-0633(09)00037-3  
DOI: doi:10.1016/j.pss.2009.01.011  
Reference: PSS 2622

To appear in: *Planetary and Space Science*

Received date: 7 July 2008  
Revised date: 11 December 2008  
Accepted date: 26 January 2009

Cite this article as: C.J. Howe, D. Drummond, R. Edeson, B. Maddison, D.J. Parker, R. Parker, A. Shrivastava, J. Spencer, B.J. Kellett, M. Grande, P. Sreekumar, J. Huovelin, D.R. Smith, J. Gow, S. Narendranath.K.C. and L. d'Uston, Chandrayaan-1 X-ray spectrometer (C1XS) – Instrument design and technical details, *Planetary and Space Science* (2009), doi:10.1016/j.pss.2009.01.011

This is a PDF file of an unedited manuscript that has been accepted for publication. As a service to our customers we are providing this early version of the manuscript. The manuscript will undergo copyediting, typesetting, and review of the resulting galley proof before it is published in its final citable form. Please note that during the production process errors may be discovered which could affect the content, and all legal disclaimers that apply to the journal pertain.



[www.elsevier.com/locate/pss](http://www.elsevier.com/locate/pss)

**Title:** Chandrayaan-1 X-ray Spectrometer (C1XS) – Instrument Design & Technical Details

**Authors:** C.J. Howe, D. Drummond, R. Edeson, B. Maddison, D.J. Parker, R. Parker, A. Shrivastava, J. Spencer, B.J. Kellett, M. Grande, P. Sreekumar, J. Huovelin, D. R. Smith, J. Gow, S. Narendranath.K.C. & L. d’Uston.

\* Corresponding author: Chris J. Howe [c.j.howe@rl.ac.uk](mailto:c.j.howe@rl.ac.uk)

Tel: +44 (0)1235 445016

Fax: +44 (0)1235 445848

---

*Manuscript number: PSS954*

*Submitted to Planetary and Space Science on 7 July 2008*

*re-submitted on 12 Dec 2008*

*Editor: Meta Ottevangner*

# 1 Chandrayaan-1 X-ray Spectrometer (C1XS) – Instrument Design & Technical Details

2  
3 C.J. Howe<sup>a,\*</sup>, D. Drummond<sup>a</sup>, R. Edeson<sup>a</sup>, B. Maddison<sup>a</sup>, D. J. Parker<sup>a</sup>, R. Parker<sup>a</sup>, A.  
4 Shrivastava<sup>b</sup>, J. Spencer<sup>a</sup>, B.J. Kellett<sup>a</sup>, M. Grande<sup>d</sup>, P. Sreekumar<sup>b</sup>, J. Huovelin<sup>f</sup>, D. R. Smith<sup>e</sup>,  
5 J. Gow<sup>e</sup>, S. Narendranath.K.C. <sup>b</sup> & L. d’Uston<sup>c</sup>.

6  
7  
8 <sup>a</sup> Space Science and Technology Department, Rutherford Appleton Laboratory, Didcot, Oxon,  
9 OX11 0QX, UK.

10 <sup>b</sup> Indian Space Research Organisation, Bangalore, India.

11 <sup>c</sup> Centre d’Etude Spatiale des Rayonnements, CNRS/UPS, Toulouse, France.

12 <sup>d</sup> Institute of Mathematical and Physical Sciences, University of Wales, Aberystwyth.  
13 Ceredigion, SY23 3BZ, UK.

14 <sup>e</sup> Imaging for Space and Terrestrial Applications Group, School of Engineering and Design.  
15 Brunel University, Uxbridge, Middlesex, UB8 3PH, UK.

16 <sup>f</sup> Observatory, P.O. Box 14, FI-00014, University of Helsinki, Finland.

17  
18 \* Corresponding author : Tel : +44 (0)1235 445016 ; fax : +44 (0)1235 445848

19 Email address: c.j.howe@rl.ac.uk

## 22 Abstract

23  
24 The UK-built Chandrayaan-1 X-Ray Spectrometer (C1XS) is flying as an ESA instrument on  
25 India’s Chandrayaan-1 mission to the Moon. The Chandrayaan-1 mission launched on the 22<sup>nd</sup>

26 October 2008 and entered a 100 km polar lunar orbit on the 12<sup>th</sup> November 2008. C1XS builds  
27 on experience gained with the earlier D-CIXS instrument on SMART-1, but will be a  
28 technically much more capable instrument. Here we describe the instrument design.

29

30 *Keywords:* Detectors; SCD; Swept Charge Device; X-ray Fluorescence; Moon

31

32

### 33 **1. Introduction**

34

35 The Chandrayaan-1 X-ray fluorescence Spectrometer (C1XS) is based upon the successful  
36 technology demonstration D-CIXS instrument that was flown on the ESA SMART-1 mission  
37 (*Grande et al., 2003; 2007*). The restructured C1XS instrument design had to take into  
38 account the different thermal environment, the shorter Earth-Moon transit time, and the lower  
39 lunar orbit of the Chandrayaan-1 mission compared to the SMART-1 mission. The scientific  
40 objectives of this instrument, which include mapping the abundances of the major rock-  
41 forming elements (principally Mg, Al, Si, Ti, Ca and Fe) in the lunar crust are discussed by  
42 Crawford et al., (*in press*). Here we describe the instrument design and technical challenges  
43 presented by the C1XS instrument which uses innovative swept charge device (SCD) detector  
44 technology (*Grande et al., 2003; Holland et al., 2004; Smith et al., 2007*).

45

46 The C1XS instrument, like its predecessor, will be accompanied by a X-ray Solar Monitor  
47 (XSM) instrument.

48

### 49 **2. XSM Instrument**

50

51 The XSM is very similar to the instrument for SMART-1 described in *Huovelin et al. (2002)*  
52 and *Alha et al. (2008)*. It consists of an aluminium enclosure containing a high purity silicon  
53 PIN (Positive Intrinsic Negative) diode detector, a Peltier cooler, front end electronics, and a  
54 shutter mechanism (Fig.1). The signal processing card is fitted inside the C1XS electronics  
55 module; the data produced is read by the C1XS processor, assembled into 512 bin spectra and  
56 transmitted to the spacecraft solid state recorder (SSR).

57

58 The PIN diode is formed on a square chip and has a circular active area. Three concentric  
59 guard rings surround the active detection area. To reduce the count rate an aperture stop made  
60 from a golden annular structure is centred on the surface of the detector. The detector window  
61 consists of a 13  $\mu\text{m}$  beryllium foil coated with 0.25  $\mu\text{m}$  polyimide and 90 nm aluminium. A  
62 collection of the XSM performance values are shown in Table 1.

63

64 The main differences from the SMART-1 XSM are: (1) improvement in the noise performance  
65 implying better spectral resolution as well as a lower energy cut-off, and (2) a smaller aperture  
66 resulting in decreased sensitivity to allow measurements of spectral signature of very strong  
67 flares.

68

### 69 **3. C1XS Instrument**

70

71 2 and Fig. 3) weighs 5.56 kg and has physical dimensions of approximately 250 mm wide by  
72 150 mm tall by 190 mm deep (with the door closed). It is functionally and thermally divided  
73 into two parts. The larger section is the electronics module. This module contains the  
74 instrument main power switching and conditioning circuits, the switched mode power supply  
75 and five circuit boards. The circuit boards are arranged side-to-side, and are held in place with

76 wedge-locking card guides. The electronics enclosure is a thick-walled (4 mm) aluminium  
77 box, which acts as the instrument's primary structure. The second section is the detector  
78 module. This houses the swept charge device (SCD) X-ray detectors together with their  
79 associated drive electronics, radiation shielding and cooling interface. It is supported by the  
80 electronics module in a cantilever fashion.

81

82 The instrument (Fig. 1) weighs 5.5 kg and the instrument is bolted down to the Chandrayaan-1  
83 spacecraft deck using 4 screws to provide a good thermal interface between the instrument and  
84 the spacecraft panel/radiator. Table 2 gives a list of requirements together with the actual  
85 values measured during the C1XS calibration and test.

86

### 87 **3.1 Overview of C1XS Instrument Operation**

88

89 C1XS uses a form of Charge Coupled Device (CCD) developed by e2v specifically to detect  
90 X-rays. When an X-ray in the 0.5 to 20 keV energy range arrives at the device it deposits a  
91 charge which is proportional to the energy of the X-ray. This charge is read by the C1XS and  
92 converted to a digital amplitude value. (Detail of how the detectors operate is provided in  
93 more detail in section 3.3.) The digital value is compared with a software configured threshold,  
94 any event above the threshold is considered to be a valid X-ray event (see section 3.4). The  
95 validated event is either assembled into a data packet or used by the C1XS data processing  
96 system to create a spectrum for each SCD. The generated spectrum is made up of 512 energy  
97 bins, for each event the C1XS software calculates within which energy bin the event would fall  
98 and increments that bin's number of counts. Every 8 seconds each SCD spectrum is assembled  
99 into a data packet and the bin counters are reset to zero.

100

### 101 3.2 Detector Module

102

103 The detector module is mounted on the front of the electronics module via a 12 mm thick  
104 GFRP (glass fibre reinforced polymer) spacer. The heads of the bolts used to hold the two parts  
105 together are also insulated from the detector module. The GFRP spacer is covered with  
106 stainless steel foil, designed to provide electromagnetic shielding without adding a significant  
107 thermal connection. The void between the 2 modules is filled with a 10 layer multi-layer  
108 insulation (MLI) blanket to reduce the radiative coupling between the hot video processing  
109 electronics and the back of the cold detectors. The electrical interface between the two parts is  
110 via a flexi-rigid circuit board which has been designed to minimise heat transfer (Fig. 3).

111

112 The SCD clock driver PCB (printed circuit board) is fixed to the rear of the detector module  
113 and contains the power drive stages for the SCD clocks and the interface connectors for the  
114 SCD modules. There are 3 SCD modules, each with an interface PCB. Each module contains  
115 two strips of SCDs with 4 SCDs in each strip. The SCD strips are mounted on a 3 mm copper  
116 and a 6 mm tantalum heatsink, which is thermally isolated from the rest of the module. The  
117 tantalum is included for proton shielding but also provides additional thermal mass. The  
118 copper protrudes from the bottom of each SCD module to allow the external radiator to be  
119 connected to the instrument via a heatpipe (Fig. 3).

120

121 To constrain the detector field of view, a CNC (computerised numeric control) machined  
122 copper collimator (Fig. 4) is mounted above each detector. This provides an angular acceptance  
123 of  $28^\circ$  (i.e.  $\pm 14^\circ$ ) from the 100 km orbit of Chandrayaan-1, the C1XS field of view being  
124 equivalent to a 50 km square (full width) on the surface of the Moon. The dimensions of the  
125 machined holes in the copper are 1.5 mm square with a wall thickness of 0.15 mm. The signal

126 loss due to the copper walls is just 17 %. This is a superior performance to the D-CIXS  
127 collimators which lost ~30%. To allow the walls to be made this thin the maximum machining  
128 depth is 1 mm. Therefore, a complete collimator is composed of six machined copper sheets  
129 stacked up to give the necessary opening angle. As part of the CNC process extra holes are  
130 machined to allow the individual sheets to be accurately aligned and fixed together to ensure  
131 correct construction of each collimator stack.

132

133 SCDs are not just sensitive to X-rays; light and low energy electrons can also mimic an X-ray  
134 signal. A 0.2  $\mu\text{m}$  aluminium foil supported on 0.2  $\mu\text{m}$  polyimide is therefore mounted to the  
135 top and bottom layers of the collimator stack. The reason for having two thin foils rather than  
136 one thicker foil is to eliminate possible problems with pin-hole defects in the foils. It is very  
137 unlikely that an individual column would have a pin-hole present in both of the foils and even  
138 less likely that the two holes would line up to provide a light path through to a detector. One of  
139 the internal collimator layers has additional vent paths included to ensure that the trapped  
140 volume of air does not cause the aluminium foil to rupture during the decompression  
141 experienced during the launch. The vent paths are designed to reduce the possibility of light  
142 entering one collimator getting to another if the external foil is ruptured. Unlike D-CIXS where  
143 seven of the detectors were mounted behind a magnesium foil collimator assembly (*Grande et*  
144 *al., 2003*), the new C1XS instrument only employs aluminium foils. A photograph of a partly  
145 built collimator stack and a schematic of the collimator assembly are shown in Figure 4.

146

147 The entire detector module is protected by a 5 mm thick aluminium door. This door is actuated  
148 with a stepper motor, using a rotary potentiometer for control. DCIXS used microswitches at  
149 each end of the door's travel and so the precise door position was never known. The  
150 potentiometer fitted to C1XS will allow the door position to be measured at all times. The



151 door is secured for launch using a one-shot HOP wax actuator and contains 24  $^{55}\text{Fe}$  sources for  
152 calibrating the detectors when closed.

153

154 Each  $^{55}\text{Fe}$  calibration source consists of a 220 kBq nickel coated electro-deposited source on an  
155 aluminium carrier which is mounted behind a 5  $\mu\text{m}$  titanium foil. The titanium is used to  
156 produce an additional pair of calibration lines so the source gives a total of four X-ray energies;  
157 4.510, 4.931, 5.895 and 6.4942 keV corresponding to the K-alpha and K-beta lines of Ti and  
158 Mn, respectively.

159

160 The source and foil are mounted in a holder, which is used to restrict the source viewing angle  
161 so that the measurements from the lunar surface are not 'contaminated' with the X-rays emitted  
162 by the calibration sources. Due to the titanium foil and the collimation the count rate seen by  
163 each detector is approximately 200 counts per second. At the beginning of the mission 10  
164 minutes of calibration data will be taken once per day to monitor the SCD degradation, the  
165 time may be lengthened as the mission progresses due to the source half life (2.7 years).

166

### 167 **3.3 Swept Charge Devices and Drivers**

168

169 A schematic of the SCD internal structure is given in Figure 4 and the device characteristics,  
170 specified by the supplier, are given in Table 3. The device has 3 clock lines which are  
171 arranged in a design that, upon clocking, will 'sweep' any charge towards a low capacitance  
172 sense amplifier located in one corner of the detector (the bottom left-hand corner as shown in  
173 Figure 5). The device is clocked continuously at 87 kHz using a 10 V drive level, the clock  
174 waveforms produced by the field-programmable gate array (FPGA) are non-overlapping and  
175 the design relies on the SCD internal capacitance and a series resistor to ensure that sufficient

176 overlap is present to give correct charge transfer. Switching the clocks simultaneously  
177 substantially reduces clock noise feedthrough leading to a significant improvement in detector  
178 performance. Using a lower clock frequency than that specified by the manufacturer increases  
179 the theoretical dark current by approximately 2 electrons per sample.

180

181 The design of the sense amplifier is based upon that used in traditional CCD technology,  
182 consisting of a very low capacitance sense amplifier and reset transistor, and operates in  
183 exactly the same way as in a conventional CCD. The SCD supply voltages are listed in Table  
184 4. All 24 SCD use the same supply and clock voltages to minimise the complexity of the drive  
185 electronics and because the 24 SCD are contained on 6 substrates each of which has common  
186 bias voltage and clock connections. As part of the characterisation work done by Brunel  
187 University, the SCD drive voltages and biases were investigated in detail and it was found that  
188 all the flight candidate devices could perform well under a single set of optimised voltages.  
189 Figure 6 shows one parameter investigated in the study, the variation in noise as a function of  
190 output drain voltage. All the devices used in the final flight instrument were characterised  
191 using the specified optimal voltages and were the ‘best’ modules chosen for those operating  
192 conditions.

193

194 The four SCD bias voltages and logic-level clocks are generated on the video-digital PCB and  
195 are connected to the SCD via the video-analogue card. The clock driver board is mounted  
196 directly on the detector assembly module and uses flexi-rigid circuits to connect to the  
197 analogue card. Different flexible circuits are used to separate the drive waveforms/supplies to  
198 the detectors from the SCD video outputs to minimise interference.

199

200 The clock driver board carries the power driver ICs (integrated circuits) for the clocks, and the  
201 connectors which allow the SCD modules to be plugged in once the rest of the instrument is  
202 assembled. The PCB on the back of the SCD module holds the SCD supply filter components  
203 to provide decoupling as close to the device as possible.

204

205 The substrate and output gate voltages for the SCDs are each generated using a DAC08 digital  
206 to analogue converter followed by a power drive stage. The remaining two voltages come  
207 from a switched-mode power supply (SMPS) which is synchronised to the SCD readout  
208 system. The output of the SMPS is filtered and then the actual output voltage selected using  
209 linear voltage regulators. Control for these voltages comes from the video processing boards.

210

### 211 **3.4 SCD Video Processing**

212

213 The signals from each SCD flow through 3 main processing blocks: video amplification and  
214 sampling, digitisation, and event recognition (Fig. 7). As the output from an SCD is similar to a  
215 conventional CCD, a correlated double sampling (CDS) circuit is used to extract the wanted  
216 signal. The CDS circuit takes two samples from the SCD for each pixel, the reset level and  
217 then the X-ray event signal, and calculates the difference between the two values. This voltage  
218 is then fed, via a summing junction, to an analogue to digital converter (ADC) which gives a  
219 14 bit number equivalent to the X-ray event energy. The summing junction allows the position  
220 of the zero voltage signal to be placed anywhere on the ADC range, in practice this position is  
221 chosen to be at a value of 350 so that when the temperature changes, both positive and negative  
222 drift of the zero position can be detected. The instrument uses a total of 24 SCD, each  
223 requiring its own CDS circuit, so an integrated solution is required to allow all the parts to be  
224 fitted on the Eurocard sized PCB. A Burr Brown 3 channel CDS integrated circuit was chosen

225 as the main processing element. Four of these devices plus support logic were built into a  
226 module produced by 3D Plus and supplied by CESR with the support of CNES (Fig. 8). As the  
227 CDS parts are designed for optical CCD signals a pre-amplifier stage is used immediately  
228 before the CDS block to give sufficient resolution. The amplifiers have an enable input which  
229 is used to blank out the SCD reset pulse.

230

231 Each 3D Plus module, containing the CDS, is controlled using an Actel RTAX250 FPGA.  
232 This device provides the sequencing of detector readout and digitisation. It also is used to  
233 select valid X-ray events from the detector video streams. The event-selection logic stores  
234 samples from each detector and processes them according to a programmable criterion using  
235 two thresholds. The thresholds are selected such that X-ray events less than  $\sim 800$  eV are  
236 rejected by the system (threshold one). Threshold two is used to reject events where a single X-  
237 ray is spread over two or more pixels. The two event selection modes used by C1XS (Fig.9)  
238 are:

239

240 1. ‘Multi-pixel’ mode – on pixel B greater than threshold 1, up to 5 consecutive pixels  
241 (hatched area) are stored in the FIFO.

242

243 2. ‘Single pixel’ mode – on pixel B greater than threshold 1, and both A and C less than  
244 threshold 2, store pixel B (crosshatched area).

245

246 In addition, on demand from the instrument processor, the FPGA can store one raw data  
247 sample from each detector without reference to the programmed thresholds which gives an  
248 event value somewhere within the ADC range. As the read-out rate for each detector is  $\sim 87$   
249 kHz and the highest expected X-ray event rate is 900 events per second (X10 flare conditions)

250 the probability that the value read is an X-ray is 0.01. Therefore a non-thresholded event is  
251 most likely to be a measure of the system noise with respect to a zero energy value. The  
252 instrument software integrates these data to give a value of the zero energy position and adjusts  
253 the FPGA event thresholds accordingly. In addition these data are added to the telemetry  
254 packets transmitted from the instrument and are used to keep a check on the front-end analogue  
255 offsets which determine the zero-energy position in the accumulated X-ray spectra. All the  
256 validated X-ray events are stored in a FIFO which is read by the C1XS micro-controller 32  
257 times per second. It is impossible to distinguish FPGA events generated by genuine X-rays  
258 from events related to the penetrating particle background. However, by using the measured  
259 spectra from very quiet solar conditions (<B1 GOES X-ray flux level), we can determine a  
260 background spectrum which can be used to remove the cosmic ray induced X-ray signal.

261

### 262 **3.5 Data Processing System**

263

264 Figure 10 shows a block view of the C1XS data processing system. An RTX2010  
265 microcontroller is used for the main instrument processing. It is located on one of the plug in  
266 PCBs together with 256 kBytes RAM, 128 kBytes fuse linked PROM (programmable read  
267 only memory) and 256 kBytes EEPROM (electrically erasable read only memory). The  
268 software is written in a mixture of assembler and C code and has two main parts; the first is an  
269 emergency level system that allows basic communication with the instrument, the ability to  
270 read and modify RAM, start execution at a specific memory location and to boot from  
271 EEPROM having validated the integrity of the software to be run. The second part is the main  
272 instrument software which is run after the C run-time system has initialised. The instrument  
273 boots into 'Standby' mode which allows full commanding via the databus and produces  
274 housekeeping data every 64 seconds. The Standby mode functions include the following:

275

276

- C1XS Door open/close

277

- Collect and transmit instrument operating parameters

278

- Synchronise internal clock to spacecraft clock

279

- Accept commands

280

281 Instrument 'Operating' mode is entered via a telecommand and, on starting this mode, the  
282 software checks that certain temperatures have not been exceeded; powers on the video  
283 processing circuits and the SCD power supplies; loads various parameters into the integrated  
284 circuits and starts the XSM state machine. The state machine is used to control the operation  
285 of the XSM detector cooler, data collection and protective shutter. Some flexibility is built into  
286 operating mode which allows each of the two C1XS 3D Plus modules to be run on their own  
287 both with and without the XSM.

288

289 In the normal operating mode the C1XS telemetry data format depends on the X-ray count rate,  
290 one of three possible science formats will be chosen. If the total X-ray rate for all 24 detectors  
291 is  $<320$  events/sec then the FPGA uses the first event selection mode (multi-pixel data).

292 Although this FPGA mode allows up to 5 pixels to be selected the instrument only uses three  
293 consecutive readout events – the actual event plus the before and after events (i.e. A, B and C  
294 in Figure 9). The science telemetry packet produced contains the event time and the 3 energy  
295 values and is called '3-pixel mode'. Above 320 events/sec the FPGA uses its second mode  
296 (single pixel) so that only one pixel of data is used (event B in Figure 9). Two telemetry  
297 formats use the single pixel mode, the first is a time tagged mode where the telemetry packet  
298 contains the event time and the energy value and the second is a spectral one which is used  
299 when the count rate exceeds 800 events/sec. The spectral format is an optimised 512 channel

300 spectrum with variable bin widths to maximise the scientific return of the instrument. Spectra  
301 are generated every 8 seconds, an unprocessed spectrum generated from the on-board  
302 calibration source is shown in Figure 11. In normal operations the instrument will  
303 autonomously select the data mode itself by checking the instrument data rate every second.  
304 Alternatively, the instrument can be commanded into one of the three CIXS science modes  
305 (time tagged – 3 pixel mode, time tagged – single pixel mode or high resolution low count  
306 spectral mode). For compatibility, we can also use one of the three earlier D-CIXS science  
307 modes (simple time tagged mode, low count spectral mode or compressed low count spectral  
308 mode).

309

310 The electronics monitors the SCD temperatures, using a thermistor mounted on the rear of the  
311 SCD copper heatsink, and switches to a low power mode ('Resting') if they get too hot (~  
312 -5°C). This mode allows the detectors to cool down and data collection is re-enabled once the  
313 temperature has reduced sufficiently (to ~ -9°C).

314

315 Operating mode functions include:

- 316 ○ Monitor box and video processor temperatures, switch to standby if limit  
317 exceeded
- 318 ○ Monitor SCD temperatures, switch to low power mode (Resting) if limit  
319 exceeded
- 320 ○ Control and monitor XSM
- 321 ○ Monitor SCD X-ray event rate and generate appropriate science data packet
- 322 ○ Collect and transmit instrument and SCD operating parameters
- 323 ○ Synchronise internal clock to spacecraft clock
- 324 ○ Accept commands

325

326 Resting mode functions:

- 327       ○ Monitor box and video processor temperatures, switch to standby if limit
- 328       exceeded
- 329       ○ Monitor SCD temperatures, switch to operating mode if SCD are cool enough
- 330       ○ Collect and transmit instrument operating parameters
- 331       ○ Synchronise internal clock to spacecraft clock
- 332       ○ Accept commands

333

### 334 **3.6 Spacecraft Interface**

335

336 The C1XS instrument uses a CAN bus to communicate with the rest of the spacecraft. The  
337 CAN protocol circuits were designed and supplied by Swedish Space Corporation using Actel  
338 RT54SX32 devices. The system implemented uses two CAN busses, one which is in use and  
339 the other as a hot standby. The protocol chip automatically selects the active bus depending on  
340 the presence of a ‘use this bus’ message which is repeated every second and, if no message is  
341 received, then the device automatically uses the other bus. The spacecraft time is also sent  
342 using a specific CAN message on the bus to synchronise the C1XS instrument time to the  
343 spacecraft time.

344

345 A second Actel on the interface board is used to provide control signals for the multiplexers  
346 and analogue to digital converter and to latch the converter result. This device is also used to  
347 control the door latch drive and the door stepper motor.

348



349 The door stepper motor drive waveforms are generated under software control, this allows the  
350 actual door movement to be fine tuned to give a smooth opening/closing action and means that  
351 the door drive can be adjusted, if required, as the mission progresses. The door latch drive  
352 takes power directly from the spacecraft side of the C1XS power supply as the mechanism  
353 requires 28 V. To maintain isolation between the spacecraft and instrument grounds a pulse  
354 transformer is used to drive the power switching transistors, this has the additional advantage  
355 that a short circuit failure on the C1XS side of the transformer will not permanently activate  
356 the HOP drive.

357

### 358 **3.7 Power Supplies**

359

360 The power input to the main switched mode power supply (SMPS) is routed via a pulse  
361 activated power relay. The 30 W SMPS and accompanying filter module is used to generate  
362 the main 5 V and  $\pm 12$  V supplies. A RAL-designed PCB then contains the post SMPS filters  
363 and two additional supplies: a 1.5V rail for the XSM peltier cooler and a  $-5$  V rail for the video  
364 amplifiers. All these items are assembled onto the  $-X$  face of the C1XS box prior to the  
365 assembly of the rest of the electronics module, when the backplane is fitted.

366

## 367 **4. Calibration**

368

369 Figure 9 also illustrates the predicted performance of the D-CIXS instrument after 15 months  
370 of radiation damage during transit to the Moon. The performance is greatly degraded by  
371 radiation damage from the trapped protons in Earth's radiation belts encountered on the long  
372 journey time to the Moon. In contrast, Chandrayaan-1 will arrive at its destination lunar orbit  
373 within one week, resulting in much greater spectral performance at the start of the mission

374 (*Smith et al., 2007*). An equally significant lesson we learned from D-CIXS is the requirement  
375 for greater detail (*in press*). The typical measured instrument readout noise is 6-7 electrons rms.  
376

377 Figure 12 also illustrates the performance of the D-CIXS instrument after 15 months of  
378 radiation damage during transit to the Moon for an equivalent input spectrum. The  
379 performance is greatly degraded by radiation damage from the trapped protons in Earth's  
380 radiation belts encountered on the long journey time to the Moon. In contrast, Chandrayaan-1  
381 has arrived at its destination lunar orbit within three weeks, resulting in much greater spectral  
382 performance at the start of the mission (*Smith et al., 2007*). An equally significant lesson we  
383 learned from D-CIXS is the requirement for greater detail in the spectrum at low energies. To  
384 address this issue, C1XS has four times the number of channels over the energy range 0 to 4.  
385

## 386 **Conclusions**

387

## 388 **5. Conclusions**

389

390 The C1XS instrument builds upon the experience gained during the build and lessons learnt  
391 during the operation of the D-CIXS instrument (*Grande et al., 2007; Swinyard et al., in press*).  
392 Table 2 details the design requirements based on the science case outlined in Crawford et al.  
393 (*in press*) and specifications from the Indian Space Research Organisation together with the  
394 actual values measured during the instrument test. The key requirement for a good scientific  
395 return from the instrument is the ability to discriminate between the aluminium and magnesium  
396 energies (240 eV) hence the better than 200 eV spectral resolution requirement. The C1XS  
397 instrument during calibration achieved a resolution of 85 eV and data from the initial lunar  
398 commissioning work shows that radiation damage during the Earth-Moon transit is minimal (<

399 30 eV) so the worst case beginning of life resolution is 115 eV, almost a factor of two better  
400 than the requirement.

401 The greatest improvement to the build process was the use of CNC to machine the collimator  
402 structures. The complete set of collimators was made within one month and each was of  
403 uniform thickness and quality - the D-CIXS parts took more than 6 months to make and  
404 suffered from poor flatness and lack of uniformity. The disadvantage of the CIXS approach  
405 was an increased collimator height (due to the larger hole size necessary to ensure that the loss  
406 due to the thicker walls was minimised). However, the CIXS collimators out-perform the D-  
407 CIXS ones because the thinner walls and larger holes lead to a factor  $\sim 2$  smaller loss of X-rays  
408 to the walls.

409

410 During D-CIXS instrument operations it was found that the SCD temperature rose very quickly  
411 as the spacecraft traversed the sunlit side of the Moon, typically the SCD temperature was  $-30$   
412  $^{\circ}\text{C}$  at the terminator crossing and the instrument went into 'resting' mode (SCD temperature of  
413  $-9^{\circ}\text{C}$ ) near the equator. The thermal performance of the new instrument is expected to be  
414 much better due to the significantly greater level of design work that has taken place to reduce  
415 the overall instrument power and to more thoroughly isolate the SCD from the electronics  
416 module. The provision of a dedicated cooling system for the SCD by Chandrayaan-1 itself  
417 should help to ensure that the operating target temperature of  $-20^{\circ}\text{C}$  is maintained for greater  
418 than 95 % of the orbital configurations.

419

420 The electronics design was improved in two ways. First, all the power supplies were changed  
421 to a switched mode design. This reduces the overall power drawn by the full instrument  
422 (helping to reduce the thermal load). Second, significantly more time was spent improving the  
423 SCD drive circuits and amplifiers to improve the readout noise performance. This has resulted

424 in a readout noise figure of 6-7 electrons rms (*Kellett et al., forthcoming*). This is about a factor  
425 of 2 better than the readout noise performance of D-CIXS.

426

Accepted manuscript

426 **References**

427 Alha L., Huovelin J., Hackman T., Andersson H., Howe C.J., Esko E. and Väänänen M.. 2008.

428 The in-flight performance of the X-ray Solar Monitor (XSM) on-board SMART-1. *Nuclear*

429 *Instruments and Methods in Physics Research Section A: Accelerators, Spectrometers,*

430 *Detectors and Associated Equipment.* Vol. 596. Issue 3. pp. 317-326.

431

432 Grande M., Anand M., Bhandari N., Cook A.C., d'Uston L., Fernandes V.A, Gasnault O.,

433 Goswami J., Howe C.J., Huovelin J., Koschny D., Lawrence D.J., Maddison B.J., Maurice S.,

434 Narendranath S., Pieters C., Okada T., Rothery D.A., Russell S.S., Sreekumar P., Swinyard B.,

435 Wieczorek M., Wilding M. *In Press.* The Scientific Rationale for the C1XS X-Ray

436 Spectrometer on India's Chandrayaan-1 Mission to the Moon. *Planetary and Space Science..*

437 *(In Press).*

438

439 Grande M., Maddison B. J., Howe C.J., Kellett B. J., Sreekumar P., Huovelin J., Crawford I.

440 A., Duston C. L., Smith D., Anand M., Bhandari N., Cook A., Erd C., Fernandes V., Foing B.,

441 Gasnaut O, Goswami J.N., Holland A., Joy K. H., Kochney D., Lawrence D., Maurice S.,

442 Narendranath S., Okada T., Pieters C., Rothery D., Russell S. S., Shrivastava A., Swinyard

443 B.M., Wieczorek M., Wilding M. Forthcoming. The C1XS X-ray spectrometer on

444 Chandrayaan-1. *Planetary and Space Science.* (Submitted Nov. 2008).

445

446

447 Grande M., Browning R., Waltham N., Parker D., Dunkin S. K., Kent B., Kellett B.,

448 Perry C. H., Swinyard B., Perry A., Feraday J., Howe C., McBride G., Phillips K., Huovelin J.,

449 Muhli P., Hakala P. J., Vilhu O., Laukkanen J., Thomas N., Hughes D., Alleyne H., Grady M.,

450 Lundin R., Barabash S., Baker D., Clark P. E., Murray C. D., Guest J., Casanova I.,

- 451 D'Uston L. C., Maurice S., Foing B., Heather D. J., Fernandes V., Muinonen K., Russell S. S.,  
452 Christou A., Owen C., Charles P., Koskinen H., Kato M., Sipila K., Nenonen S.,  
453 Holmstrom M., Bhandari N., Elphic R., Lawrence D. 2003. The D-CIXS X-ray mapping  
454 spectrometer on SMART-1. *Planetary and Space Science*. Vol. 51. Issue 6. pp. 427 – 433.  
455
- 456 Grande M., Kellett B.J., Howe C., Perry C.H., Swinyard B., Dunkin S.K., Huovelin J., Alha L.,  
457 D'Uston L.C., Maurice S., Gasnault O., Couturier-Doux S., Barabash S., Joy K.H., Crawford  
458 I.A., Lawrence D., Fernandes V., Casanova I., Wieczorek M., Thomas N., Mall U., Foing B.,  
459 Hughes D., Alleyne H., Russell S., Grady M., Lundin R., Baker D., Murray C.D., Guest J., and  
460 Christou A. 2007. The D-CIXS X-Ray spectrometer on the SMART-1 mission to the Moon -  
461 First results, *Planetary and Space Science*. Vol. 55. pp. 494-502.  
462
- 463 Holland A. D., Hutchinson I. B., Smith D. R., Pool P. 2004. Proton damage in the E2V swept  
464 charge device. *Nuclear instruments & methods in physics research*. Vol. 521. No. 2-3. pp. 393  
465 - 398.  
466
- 467 Huovelin J., Alha L., Andersson H., Andersson T., Browning R., Drummond D., Foing B.,  
468 Grande M., Hämäläinen K., Laukkanen J., Lämsä V., Muinonen K., Murray M., Nenonen S.,  
469 Salminen A., Sipilä H., Taylor I., Vilhu O., Waltham N., Lopez-Jorkama M. 2002. `The  
470 SMART-1 X-ray Solar Monitor (XSM): Calibrations for D-CIXS and independent coronal  
471 science. *Planetary and Space Science*. Vol 50. pp. 1345-1353.  
472
- 473 Kellett B. J., Narendranath S., Sreekumar P., Wallner M., Maddison B., Howe C.J., Joy K.,  
474 Weider S., Grande M. *Forthcoming*. Chandrayaan-1 X-ray Spectrometer (C1XS) – Instrument  
475 Calibration & Testing. *Planetary and Space Science*. (Submitted Dec 2008.)

476

477 Smith D.R., Gow J. and Holland A.D. 2007. Proton irradiation of swept-charge devices for the  
478 Chandrayaan-1 X-ray Spectrometer (C1XS). *Nuclear Instruments and Methods in Physics*  
479 *Research Section A: Accelerators, Spectrometers, Detectors and Associated Equipment*  
480 *Volume 583, Issues 2-3*.pp. 270-277.

481

482 Swinyard B.M., Joy K.H., Kellett B.J., Crawford I.A., Grande M., Howe C.J., Gasnault O., Fernandes  
483 V.A., Lawrence D.J., Russell S.S., Wieczorek M.A., Foing B.H., and the SMART-1 team. *In Press*. X-  
484 ray Fluorescence Observations of the Moon by SMART-1/D-CIXS and the First Detection of  
485 Ti K $\alpha$  from the Lunar Surface. *Planetary and Space Science*. (*In press 2009*).

486

487

Accepted manuscript

487 **Table Captions**

488

489 **Table 1.** XSM Parameters

490 **Table 2.** C1XS Requirements and achieved values.

491 **Table 3.** Swept Charge Device Design Specification.

492 **Table 4.** SCD Voltages.

493

494

Accepted manuscript



494 **Figure Captions**

495

496 **Figure 1.** View of the XSM instrument

497

498 **Figure 2.** View of the C1XS instrument on its vibration fixture. The door covering the SCD  
499 collimators can be identified by the radioactive warning symbol. The door HOP actuator is  
500 mounted vertically and the motor horizontally. The two connectors are the CAN bus and the  
501 XSM interfaces.

502

503 **Figure 3.** Schematic view of the C1XS instrument with one side of the instrument cut away.

504

505 **Figure 4.** Photograph of a partly built collimator stack. Schematic of the collimator assembly.

506

507 **Figure 5.** A schematic of the SCD internal structure. The electrodes are depicted by the dashed  
508 lines, whilst the charge transport channels are indicated by solid lines. The charge is swept  
509 towards the central channels and down to the output amplifier (bottom left corner) by the  
510 action of the clock signals.

511

512 **Figure 6.** Variation in SCD readout noise (electrons) with Output Drain voltage.

513

514 **Figure 7.** Block diagram showing the C1XS video processing system.

515

516 **Figure 8.** Video-analogue PCB component side view showing the two 3Dplus signal  
517 processors and associated amplifiers.

518

519 **Figure 9.** C1XS X-ray ‘single pixel’ event selection – an X-ray event is selected when pixel B  
520 is greater than threshold 1 and the pixels immediately before and after (A and C) are BOTH  
521 below threshold 2. Multi-pixel event selection – Up to 5 pixels (crosshatched area) are selected  
522 when pixel B is greater than threshold 1.

523

524 **Figure 10.** C1XS data processing block diagram.

525

526 **Figure 11.** Unprocessed Spectral Packet Data generated with X-ray events from the on-board  
527 calibration source. This shows the two  $^{55}\text{Fe}$  lines, the position of the titanium lines, the ‘zero’  
528 noise peak, the FPGA cut-off point and some ‘split’ events not removed by the FPGA event  
529 detection.

530

531 **Figure 12.** An example RESIK spectrum from a flight SCD. The red histogram (C1XS) is a  
532 spectrum combined from two measurements a Cu-Mg anode and a pure Al anode to give the  
533 three peaks seen (Cu  $L\alpha$ : 0.92 keV, Mg  $K\alpha$ : 1.25 keV, Al  $K\alpha$ : 1.49 keV). The blue spectrum is  
534 a D-CIXS equivalent low count spectrum after 15 months radiation dose. Note that the red  
535 spectrum has x4 channels to maximise the scientific return of C1XS.

536

536 **Table Captions**

537

538 **Table 2.** XSM Parameters

539 **Table 2.** C1XS Requirements and achieved values.

540 **Table 3.** Swept Charge Device Design Specification.

541 **Table 4.** SCD Voltages.

542

543

Accepted manuscript

543 **Tables**

Nominal energy range	1.2–20.0 keV
Energy resolution(BOF)	200eVat 5.9 keV
Number of spectral channels	512
FOV(circular) Diameter	104°
On-axis geometric area	0:001 cm <sup>2</sup>

544 **Table 1**

545

Accepted manuscript

545

Parameter	Requirement	Achieved
Supply voltage	28 to 42 V	20 to 45 V
Power	<10W (Standby) <30W (Operating)	6.3 W (Standby) 25.5 W (Operating)
Temperature range		As requirement
Electronics	-50 to +80 (off) -20 to +40 (operating)	
Detector module	-50 to +80 (off) -40 to +0 (operating)	
Mass	5.8 kg	5.56 kg
Dimensions (door closed)		
width (Y axis)	300 mm	248 mm
height (Z axis)	200 mm	151 mm
depth (X axis)	260 mm	190 mm
Energy Range	1 to 10keV.	0.8 to 20 keV
Field of view	<15 degrees (FWHM) <30 degrees (full angle)	14 degrees (FWHM) 28 degrees (full angle).
Spectral resolution	<200 eV at 1.25 keV.	85 eV
Readout frequency	not specified	87,381 kHz
Data volume (average)	57 Mbits/orbit	36 Mbits/orbit

546 **Table 2.**

547

548

Sensitive area:	10 x 10 mm	549
Max. Count rate:	30,000 counts/sec	550
Output noise:	3 (typ.) to 5 (max.) electrons rms. (with 100KHz Correlated Double Sampling)	551 552
Energy Resolution:	140eV at Mn $K_{\alpha}$	553
Detector Efficiency:	>30% at 280eV	554
	>30% at 10keV	555
Operating temperature:	-15°C	556

557

558 **Table 3.**

559

Accepted manuscript

559

Substrate voltage	9 V
Output Gate voltage	3 V
Reset Drain voltage	17 V
Output Drain voltage	30 V

560 **Table 4.**

561

562

Accepted manuscript

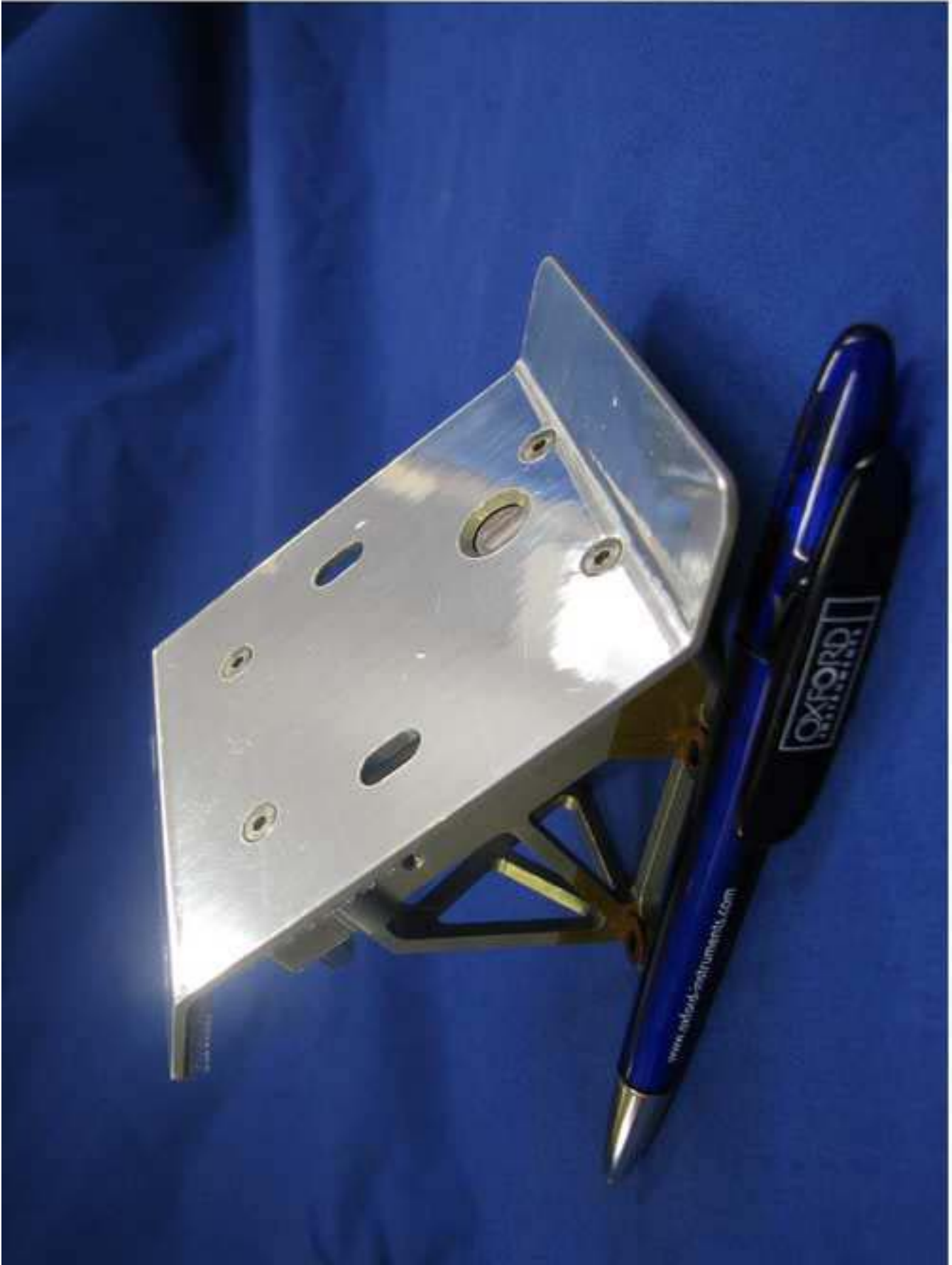


Figure 1



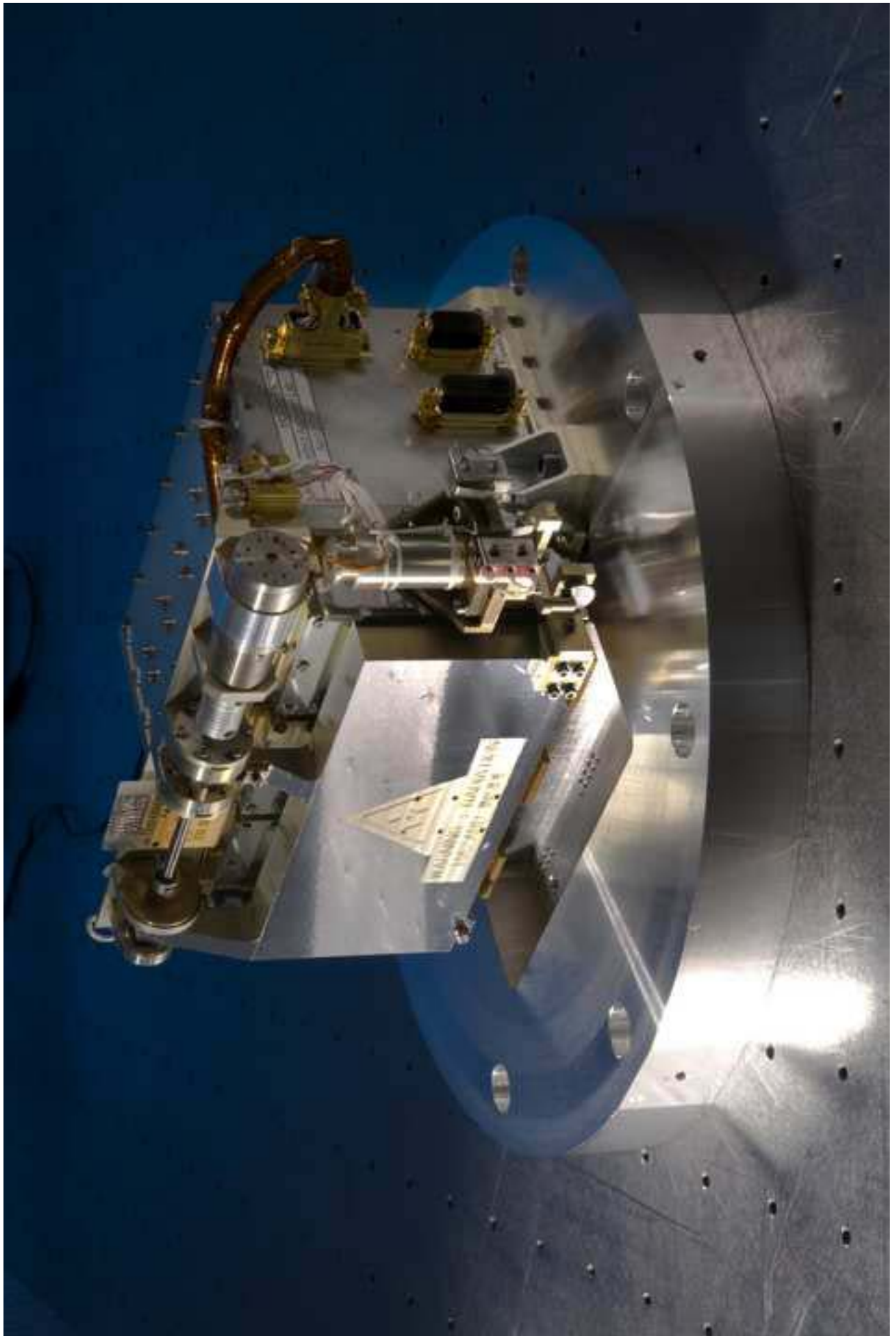


Figure 2

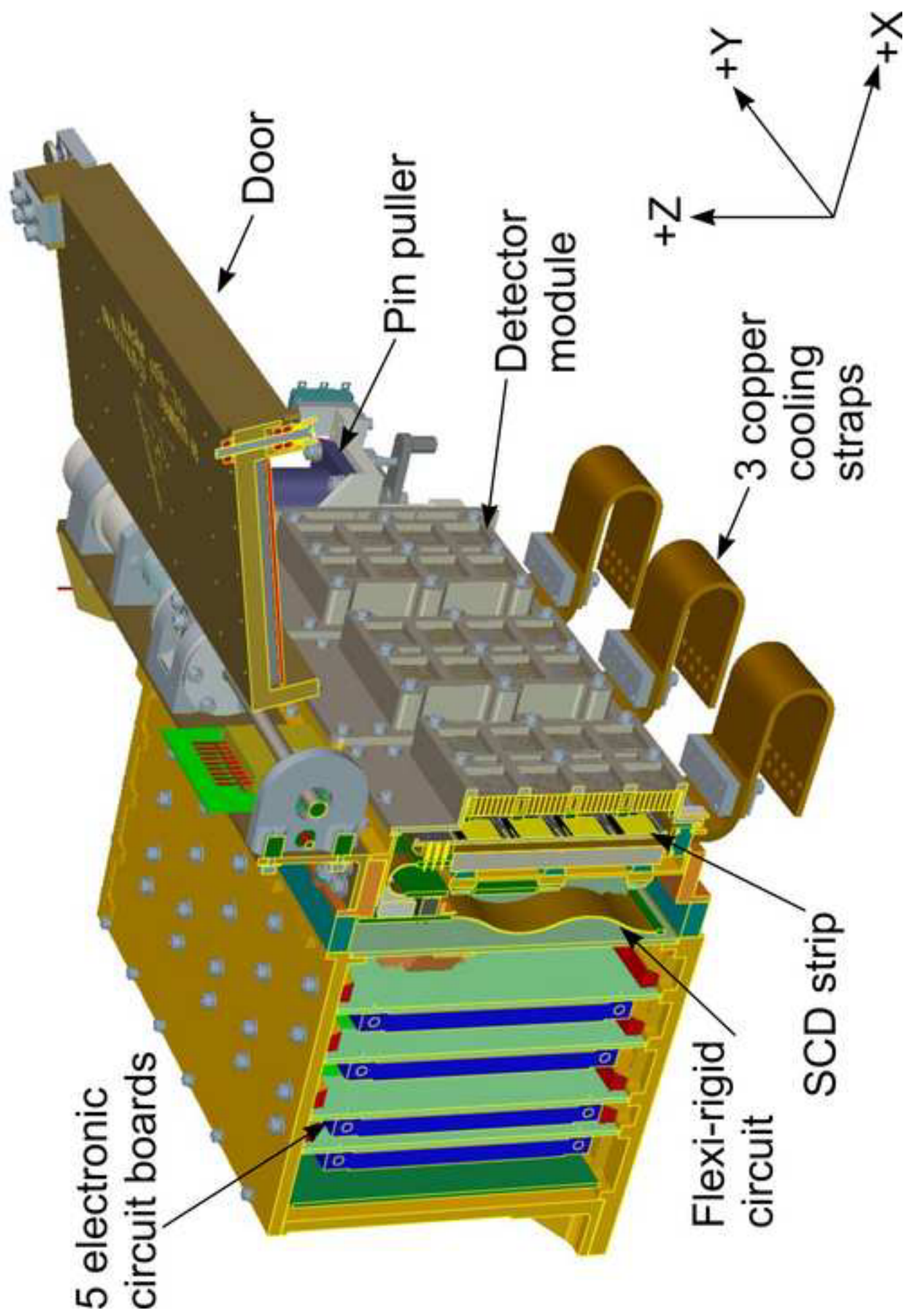
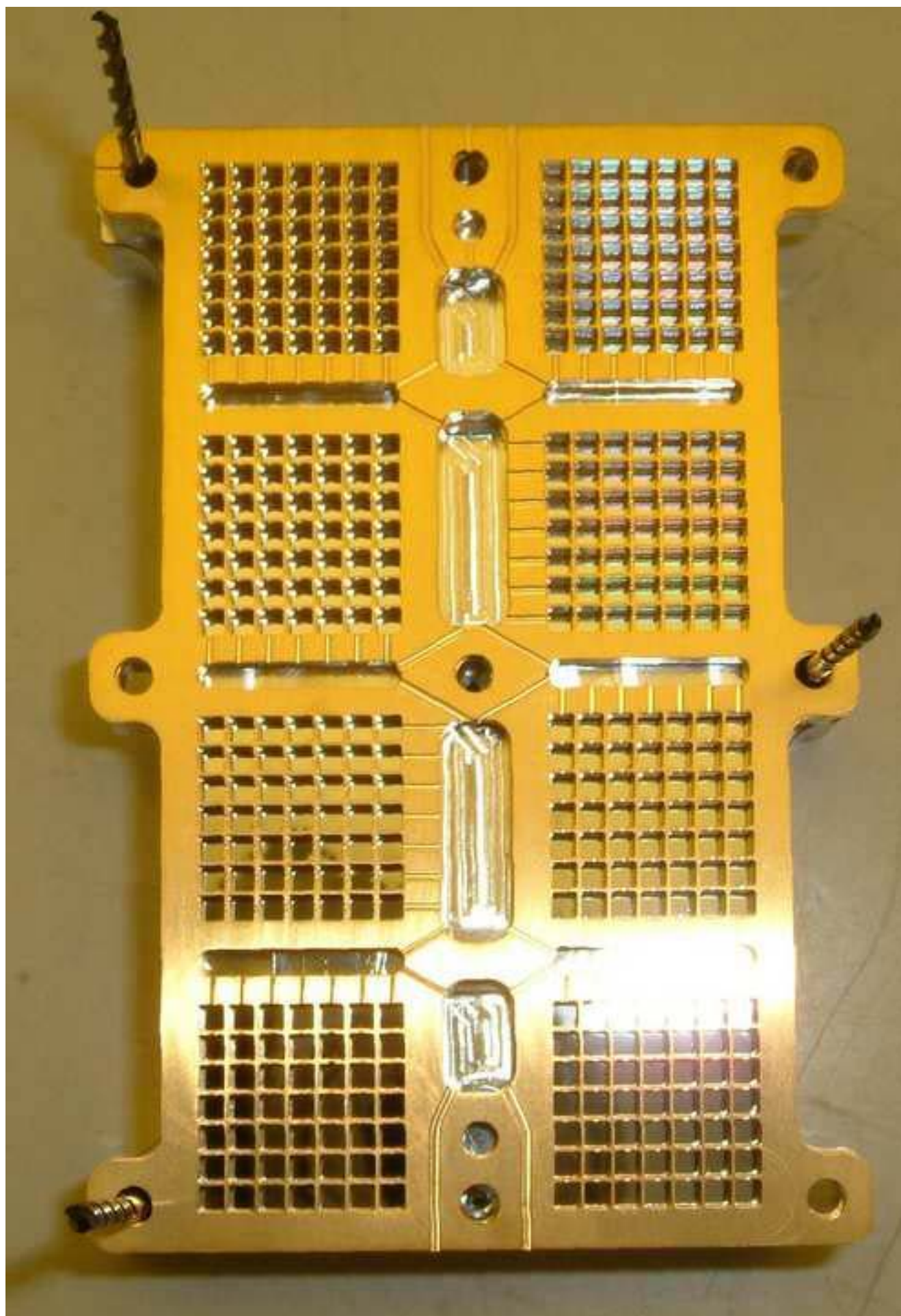
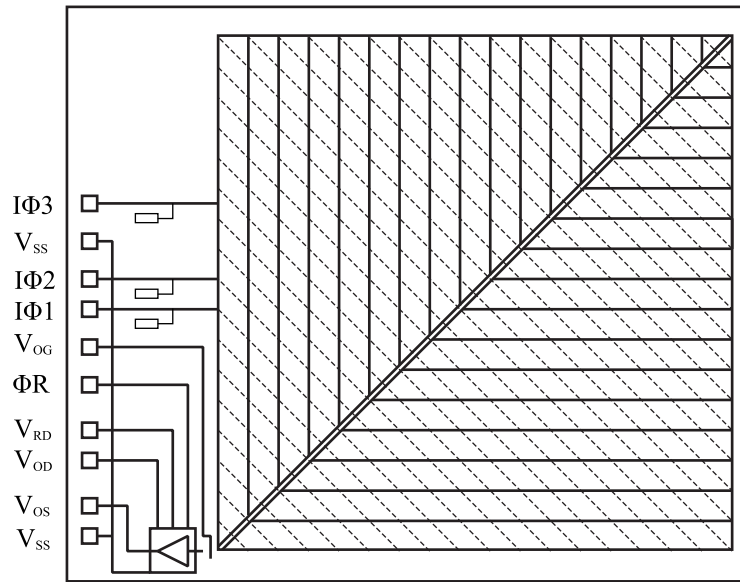


Figure 3

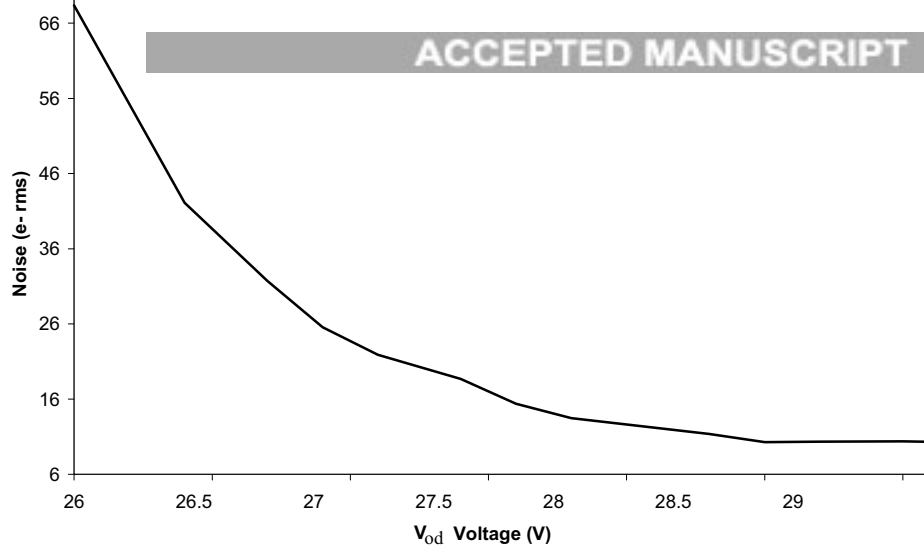
Figure 4a





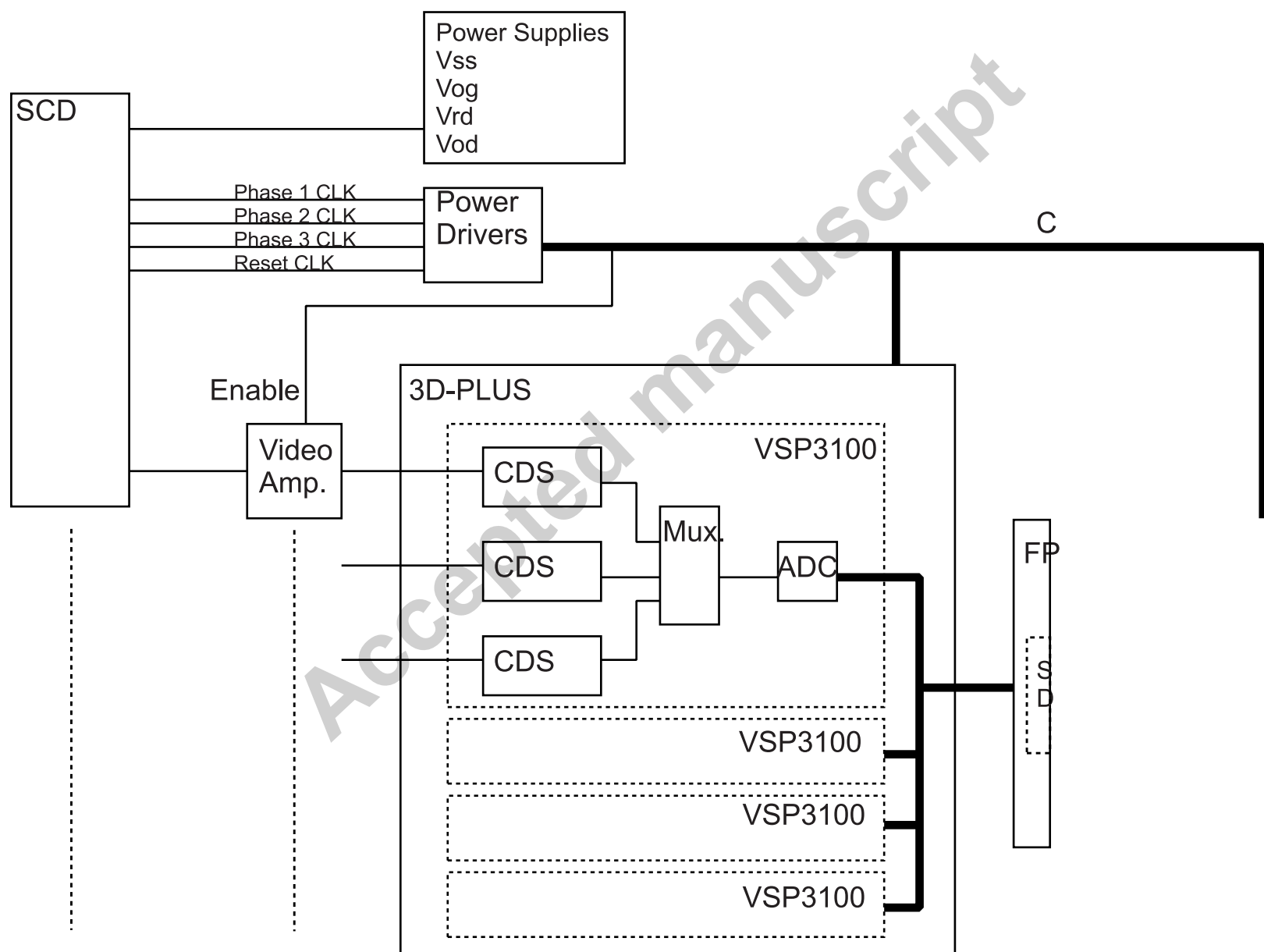
Accepted manuscript

Figure 6



Accepted manuscript

Figure 7



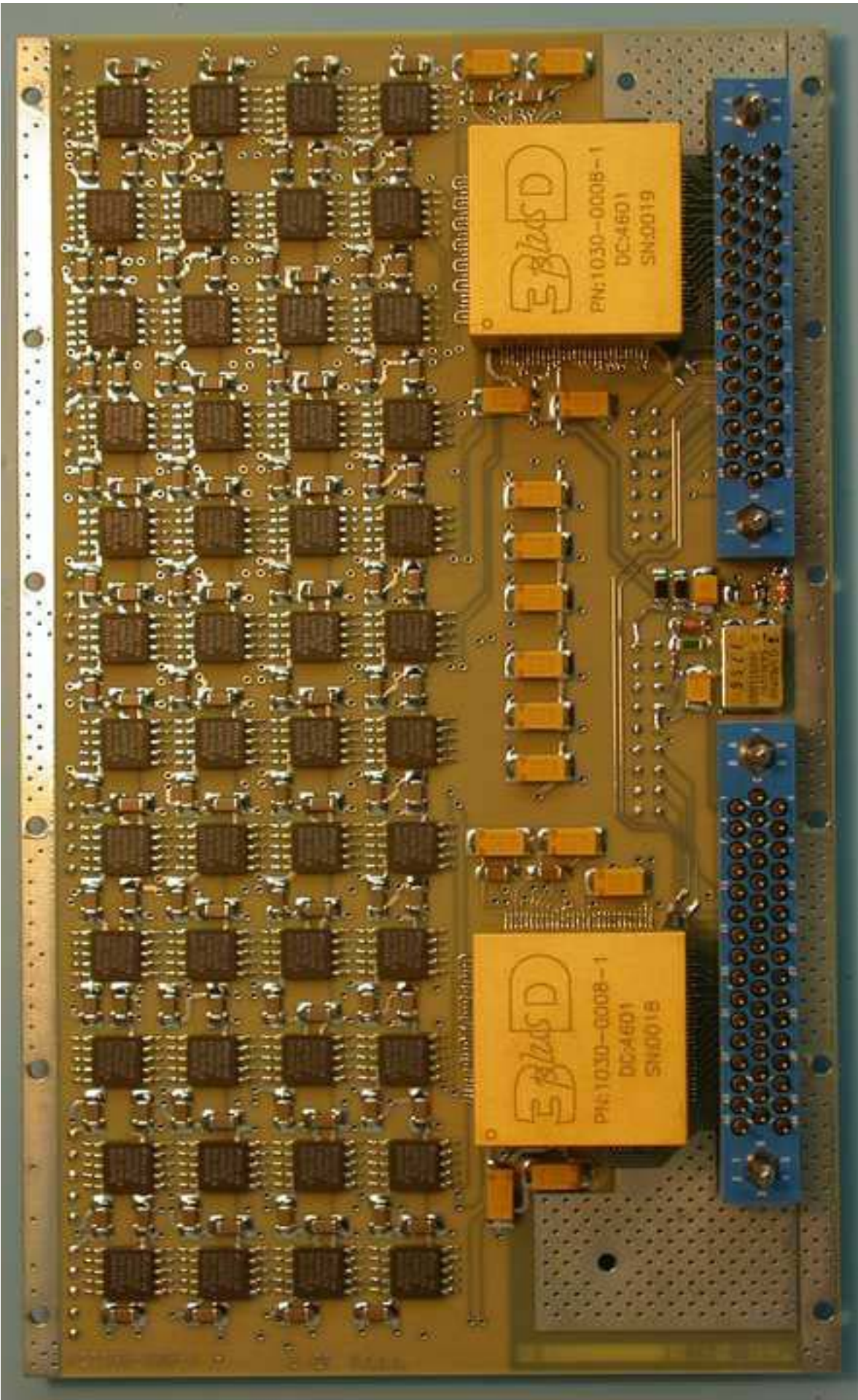
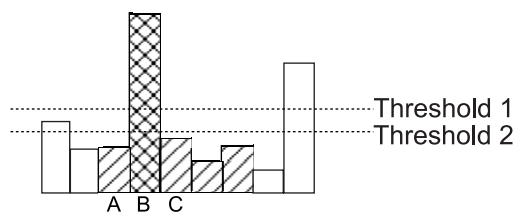


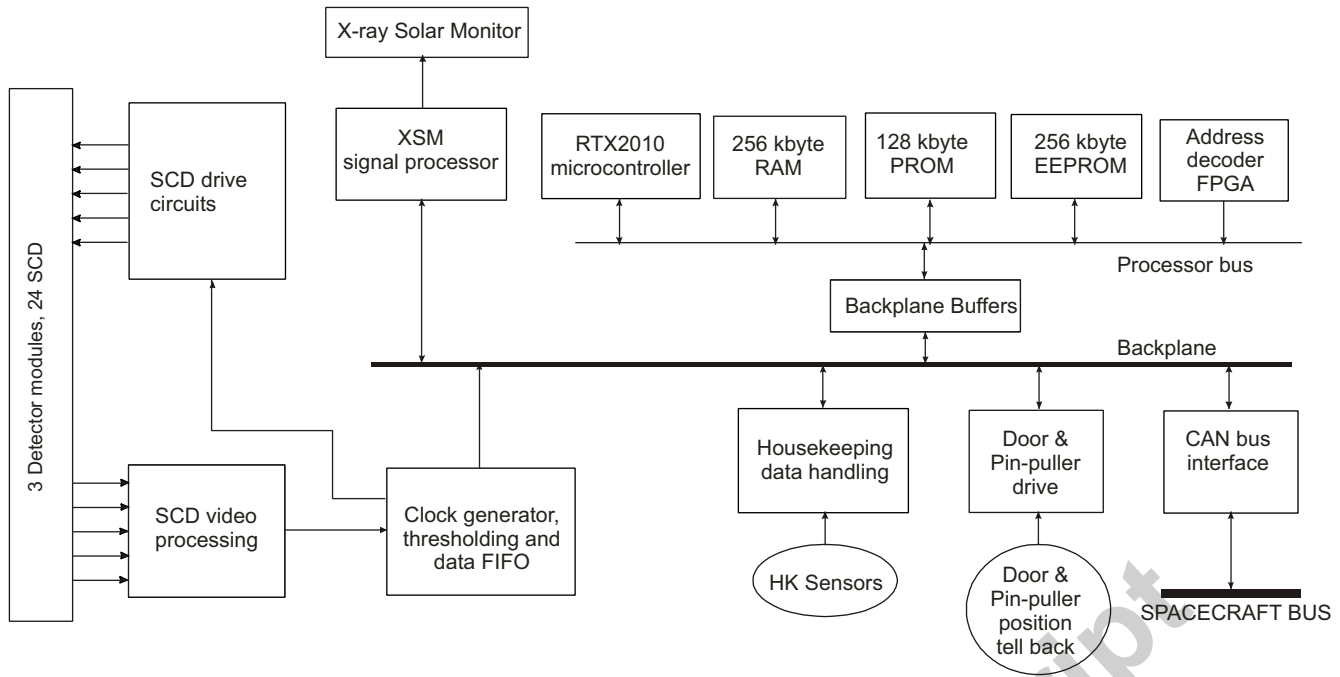
Figure 8



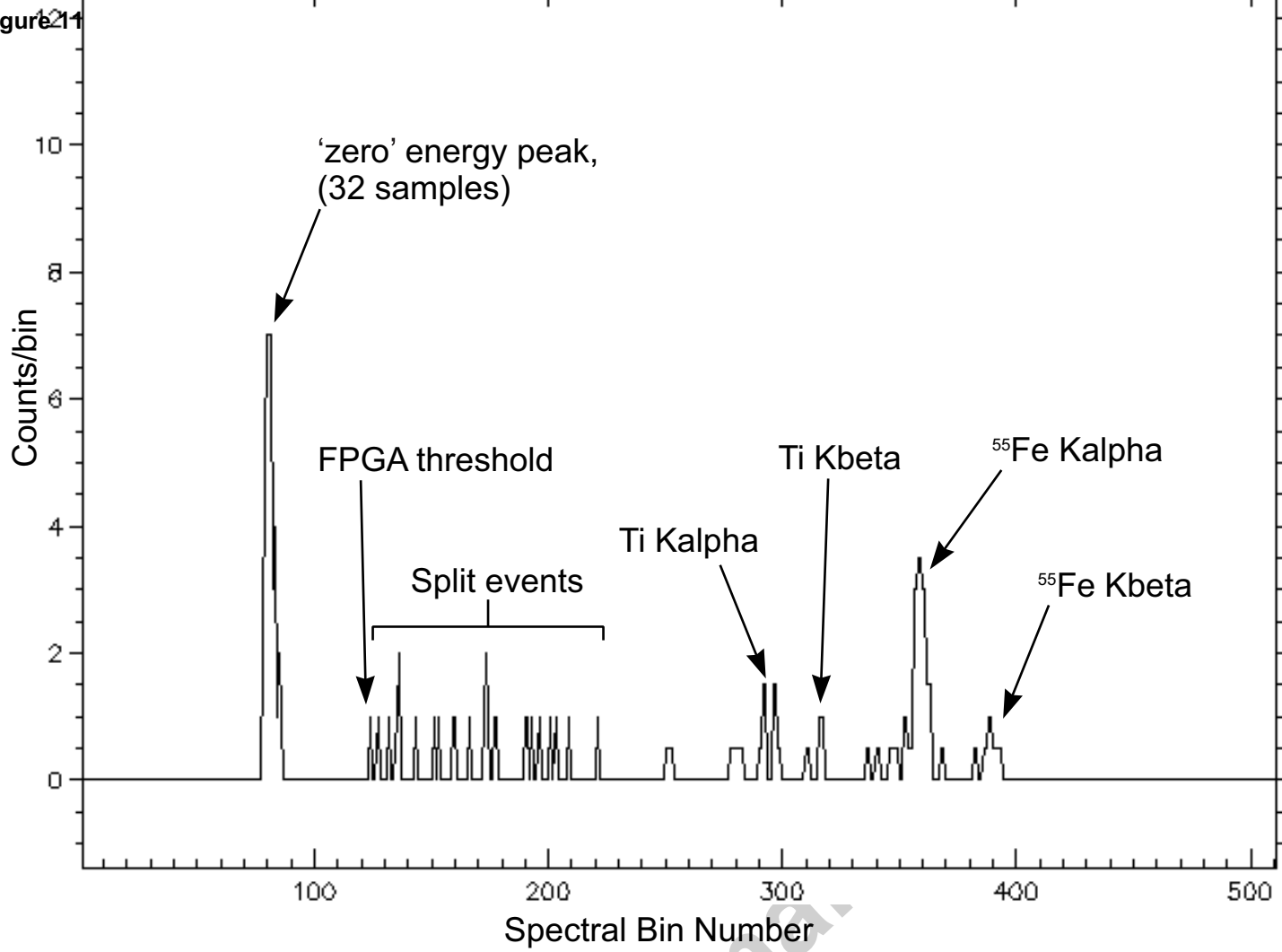
Accepted manuscript



Figure 10

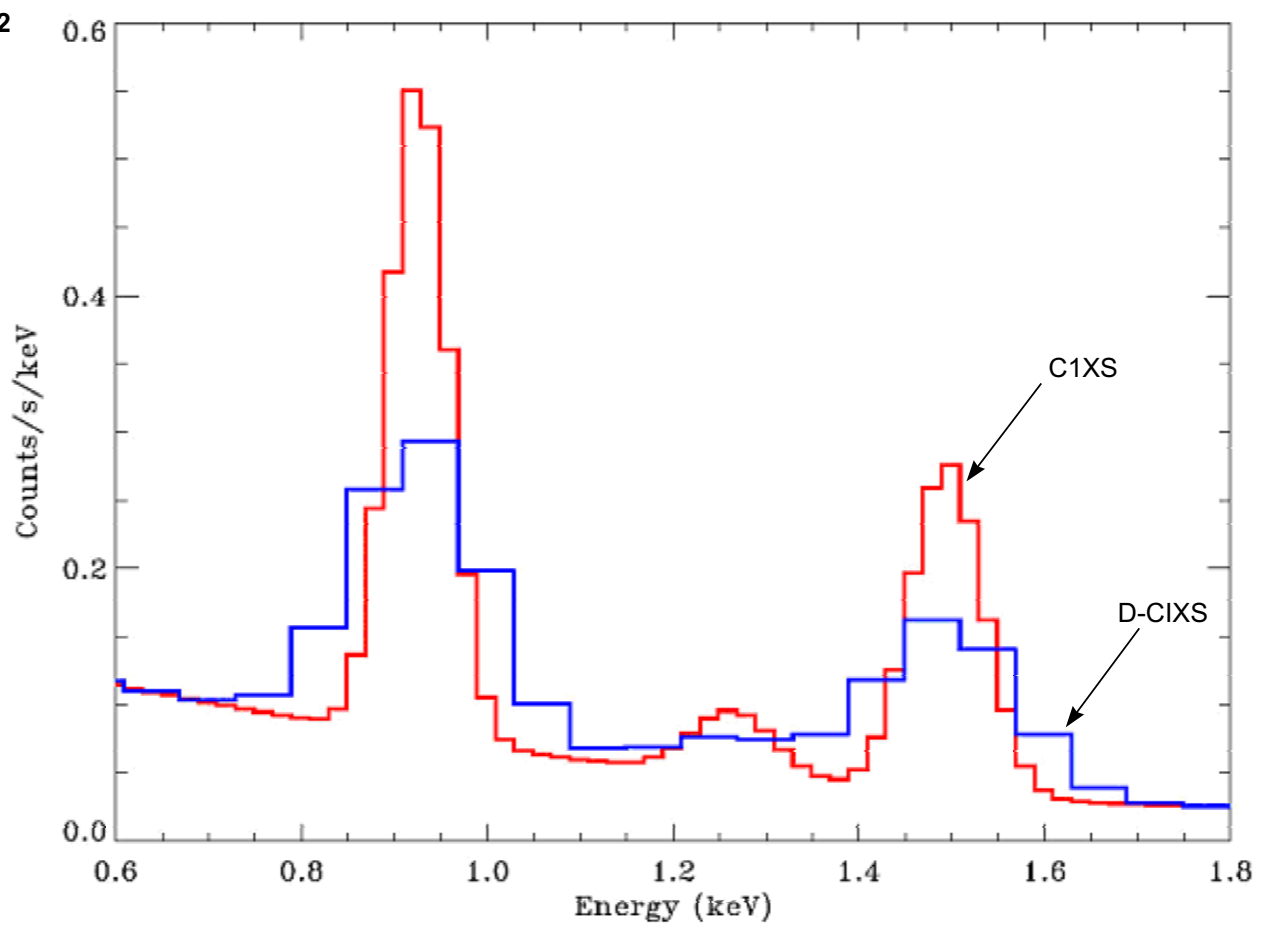


Accepted manuscript



Accepted manuscript

Figure 12



Accepted manuscript